Implementation of Travelling Waves on Lifting Surface for Drag Reduction

by

Taylor V'Dovec

Submitted to the
Department of Mechanical Engineering
in Partial Fulfillment of the Requirements for the Degree of

Bachelor of Science in Mechanical Engineering

at the

Massachusetts Institute of Technology

June 2019

Signature of Author: Signature redacted

Department of Mechanical Engineering
May 9, 2019

Certified by: Signature redacted

Dr. Micheal Triantafyllou
Professor of Mechanical and Ocean Engineering
Thesis Supervisor

Signature redacted

Accepted by:

Maria Yang
Associate Professor of Mechanical Engineering
Undergraduate Officer

Implementation of Travelling Waves on Lifting Surface for Drag Reduction

by

Taylor V'Dovec

Submitted to the Department of Mechanical Engineering
on May 11, 2019 in Partial Fulfillment of the
Requirements for the Degree of

Bachelor of Science in Mechanical Engineering

Abstract

NACA series airfoils are the standard cross-section shapes for lift-generating surfaces widely used in both aeronautic and aquatic transportation. As with any wing, the key design goal of such airfoils is to attain a large lift-to-drag ratio, namely increasing the lift force while reducing the drag force. At moderate angles of attack, boundary layer separation begins near the trailing edge, and moves up to the leading edge as the angle increases. Such a phenomenon raises the form drag significantly, and a method of pushing the separation point back towards the trailing edge could improve the overall efficiency of the foil tremendously. One such new approach is to introduce a travelling wave on the lifting surface, a technique inspired by the undulatory motion of fish. In order to manufacture and test such a surface, first the necessary design specifications must be determined. Using NACA0012 and NACA0018 wings at a Reynolds number of $1x10^5$, key parameters including the location of the point of separation on the wing, the angles of attack where the surface would be most effective, and the characteristics of the travelling wave itself were determined.

Thesis Supervisor: Dr. Micheal Triantafyllou
Tile: Professor of Mechanical and Ocean Engineering

Acknowledgements

Thank you to Dixia Fan for all your support throughout the past year. I learned so much under your guidance and had a lot of fun in the tank as well.

Thank you to Sam Calisch and Gurvan Jodin for your engineering brilliance and assistance throughout the semester.

This project would not have happened without the support of Dr. Micheal Triantafyllou and the MIT Sea Grant, as well as the MIT SuperUROP program.

As always, I could not have made it this far without the help of my loving friends and family. Thank you.

Table of Contents

List of Figures

1. Introduction

The goal for the design of any object travelling through air or water is to decrease the drag, so less thrust is needed to generate the lift required to keep the object moving. Reduced use of thrust through propulsion directly translates into fuel savings, which is a large concern for any company in transportation or shipping industries. As a result, many methods have been studied and implemented to reduce the drag force on airfoils, particularly through boundary layer control. One promising technique is the addition of travelling wave motion to trailing edge surface, which appears to push back the point of separation and reduce the form drag on the wing.[1–4] Although this idea is effective in theory, mechanical constraints make the manufacturing and installation of a moveable surface very difficult in practice. In order to implement such a device, many parameters must be taken into account, including the most effective shape and angle of attack of the wing, the ideal location of the moveable surface on the wing, and the required frequency, amplitude, and wavelength of the travelling wave. These parameters will be calculated within the laminar regime, with $Re \approx 1x10^5$.

1.1 Influence of the boundary layer on drag and lift

Many of the effects of drag take place in the boundary layer that forms on the surface of an object moving through a fluid. The two main drag components, form drag and friction drag, can both be influenced by different factors in this region. The form drag of an airfoil is dependent on the pressure gradient. As the boundary layer moves along the surface of the wing, there are both favorable and adverse pressure gradients present. A gradient of $\frac{dP}{dx} < 0$ is favorable, occurring closer to the leading edge of the wing, while adverse influences towards the trailing edge result in $\frac{dP}{dx} > 0$. Eventually, this adverse gradient slows the boundary layer enough that the velocity becomes zero, and the boundary layer no longer moves along the surface but instead detaches from the wing at a location known as the point of separation. If this transition point occurs close enough to the leading edge of the wing, no boundary layer is formed at all and the wing enters a state of stall, which is highly undesirable.

Friction drag depends on the viscous effects arising from the fluid contacting the surface of the wing. This is shown in the boundary layer by the flow triggering from laminar to turbulent. The

force exerted by laminar drag is less that that of the drag incurred when the flow becomes turbulent, so delaying this transition point is also desirable in overall drag reduction. [5]

1.2 Boundary layer control methods

With the boundary layer having such direct influence on the drag experienced by an airfoil, there have been plenty of studies done to understand its implications. Beginning with Ludwig Prandtl in the early 1900's, who was the first to hypothesize that only the friction resulting from the contact a fluid with the surface of an object has an appreciable effect, there have been many investigations into how to control boundary layer behavior. [6,7]

Basic methods that have been studied for many years include suction and riblets. Suction is initiated by slits in the wing, simply removing the slow-moving fluid at the base of the boundary layer by diverting it off the wing. This maintains the overall velocity of the boundary layer and prevents separation. [5,8]

Riblets, or patterns of raised edges on the surface of a wing, have the interesting quality of being inspired by sharks, whose skin also has ridged scales running longitudinally along the surface of their body. Although work remains to be done in this area, research has shown that this breaks up streamwise vortices and, in some turbulent applications, can reduce the drag by about 7%. [9,10]

The idea of moving the surface of airfoil itself has also been explored. This method was inspired by the behavior of rotating cylinders- on the portion of the cylinder where the external flow and the rotation are in the same direction, separation does not occur. This was further developed by Alexandre Favre, who experimented with analyzing the flow of fluids over a moving belt, and found significant increases in lift over high angles of attack. [5] He patented the addition of rollers on the trailing edge of wings, but mechanical practicalities have prevented widespread adoption. [11]

1.3 Biomimetics and drag reduction

Although research has made good headway on drag reduction, nature appears to have already solved it. The classic example is what has been found from analyses done on the boundary layers of fish. Their undulatory swimming motion has been studied for many years and has led to many attempts in measuring the drag on their bodies. The thrust and drag forces are inherently coupled in their movement, leaving rigid bodied approximations lacking. [8, 9] This inability to

accurately analyze such motion led to much speculation about how efficient they truly are. In perhaps the most famous example, early studies done by James Gray led to the conclusion that dolphins swam at a speed that would require ten times more power than they could physically produce. Although not entirely accurate, it was clear that such animals are in fact highly efficient swimmers, and it set the stage for more investigation into why this is the case. [13]

Further research has shown that a key to the drag reduction of such bodies lies in the boundary layer. Studies done on robotic fish with flexible skin show that the oscillation of the fish's body reduces the drag felt on the surface, so long as the phase speed of the body is faster than the motion of the water around it. In fact, in comparison with the same body in a rigid formation, drag was reduced by up to 50%, with a Reynolds number of $8x10^5$.[14] A detailed study of the boundary layer through video analysis on the surface of actual fish confirmed this behavior, noting travelling wave behavior that moved along the body 1.6 times faster than the motion of the full body. [2]

1.4 Mechanical challenges

Although the introduction of travelling waves on airfoils appears to be a promising way forward for boundary layer control, the difficulties arising from the implementation of such a design have led to few practical applications. The design must include a moveable surface that is able to sit flush on the wing, as protruding edges can trigger separation, and must be smooth enough to not contribute further to the friction drag. The surface must also be easily adaptable to many wing shapes, meaning it must be able to account for a slight curve in the wing due to varying thicknesses at the leading edge. Power requirements must be low enough to not offset any efficiency gains made by reducing the drag forces on the wing, and the manufactured components must have tolerances high enough to accommodate a range of frequencies at a high degree of accuracy.

In addition, there will be an optimal range of parameters at which the surface will operate best. The range of possible angles of attack where the wing is most effective is affected by many factors. At low angles, the separation point is already close to the trailing edge, and the addition of a travelling wave is unnecessary and not worth the power required. At very high angles, the flow may separate too early, and short of making the entire surface moveable, there is not much gained from boundary layer control.

The generated wave itself must also be carefully tuned. For example, if the amplitude is too high, or the frequency too low, the new surface may have no effect, or even a negative effect, and power will be wasted in the effort to activate it. These specifications will be calculated and eventually empirically tested to optimize the use of this new technology.

Through the course of this study, the point of separation for varying angles of attack was quantified in order to determine both the best location of a moveable surface on the wing and the target angles of attack that would experience the most benefit from boundary layer control. Baseline lift and drag measurements were found for the NACA0012 and NACA0018 wings of an appropriate aspect ratio ($A_R = 5.33$) for the towing tank setup, to later compare to measurements taken with the fully implemented method of separation control. The approximate frequency, wavelength, and amplitude necessary for the travelling wave to be most effective were calculated for the first iteration of the surface as well.

2. Methods

In order to determine the design requirements for such a surface, testing was done on wings of the same size and shape of the future model, minus the new technology. Although thin, cambered wings generally perform better at lower Reynolds numbers than thick, symmetric ones, the moveable surface would be unable to sit smoothly on a highly curved surface. [15] For the initial design of the wing, NACA0012 and NACA0018 airfoils were used, with NACA0018 being thicker towards the leading edge than NACA0012. High aspect ratios and endplates were utilized to enable minimal end effects.

Testing included both dye visualizations and force measurements, the former used to qualitatively determine boundary layer characteristics and the latter to quantitatively measure the drag on the wings. All testing runs took place in the MIT Towing Tank in the Parson's Laboratory, a 100 ft x 8 ft x 4 ft tank facility. All experiments were conducted at a velocity of 0.7 m/s in room temperature freshwater ($\nu = 1.0023 \times 10^{-6}$ m^2/s) for Re $\approx 1 \times 10^5$ throughout, within the laminar range. The angles of attack, α, tested for NACA0018 ranged from -3 to 16 degrees, and -3 to 14 degrees for NACA0012.

Figure 2-1: Image of NACA0018 wing in carriage. Holes in the center mark the location of the dye visualizations. Force sensors sit above and below the endcaps on the top and bottom of the wing.

2.1 Dye visualizations

A key metric in determining the effectiveness of the new wing design is the location of the point of separation of the boundary layer on the wing. In order to determine this separation point, the method of dye visualization was used. Small holes were placed on the surface on the wing, varying distances from the leading edge. Tubes were threaded through the hollow interior and set flush with the outer surface, so as the wing was pulled through the tank, colored dye flowed through tubes and into the boundary layer that formed on the surface of the airfoil. GoPro cameras were attached to the carriage to capture the behavior of the dye. Through inspection of the collected video footage, it is clear when the boundary layer separates entirely at increasing angles of attack, and the thickening of the boundary layer could also be quantified through digital analysis.

2.1.1 Qualitative boundary layer thicknesses

To approximate the boundary layer thickness at every point along the airfoils, the video results of the dye testing were analyzed. In order to measure the thickness with a higher degree of accuracy, the average value of every pixel in the video was taken throughout the course of each run, giving a smoother image of the dye on the wing. Then, the image was filtered in such a way that every pixel within a certain RGB or HGV range was reverse-masked, so only the dye, representing the boundary layer, remained. Finally, the resulting image was converted to a Boolean array, allowing the height of the boundary layer to be measured by the number of white pixels in each column of the array.

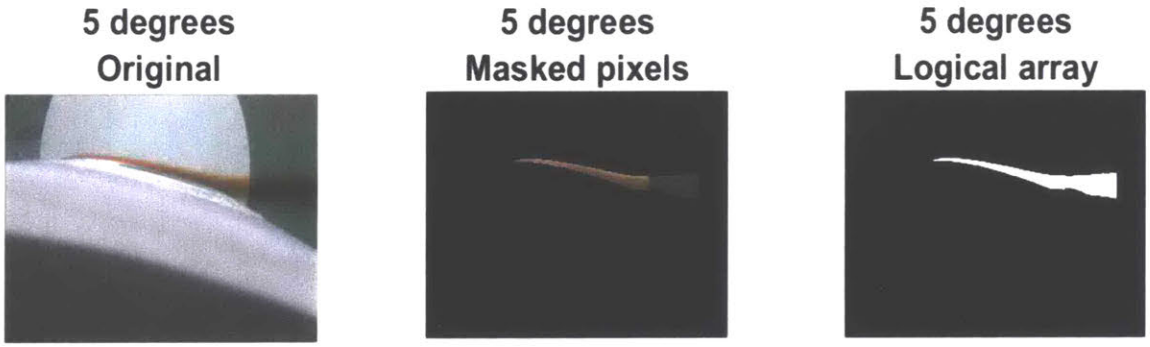

Figure 2-2 *Left* 5-degree angle of attack run with a NACA0018 wing. The pixel values throughout the footage were averaged, giving an idea of what the boundary layer looked like throughout the run without small deviations.
Center Reverse-masking of pixels, so only the dye remains in the image.
Right Logical array of the image result of the masking. The number of white pixels in the image can be summed for every x-position along the surface of the wing.

When these steps were taken at every angle of attack run in the experiment, the increase of boundary layer thickness both in the x-direction along the surface of the wing and the overall thickness at higher angles of attack was visually apparent.

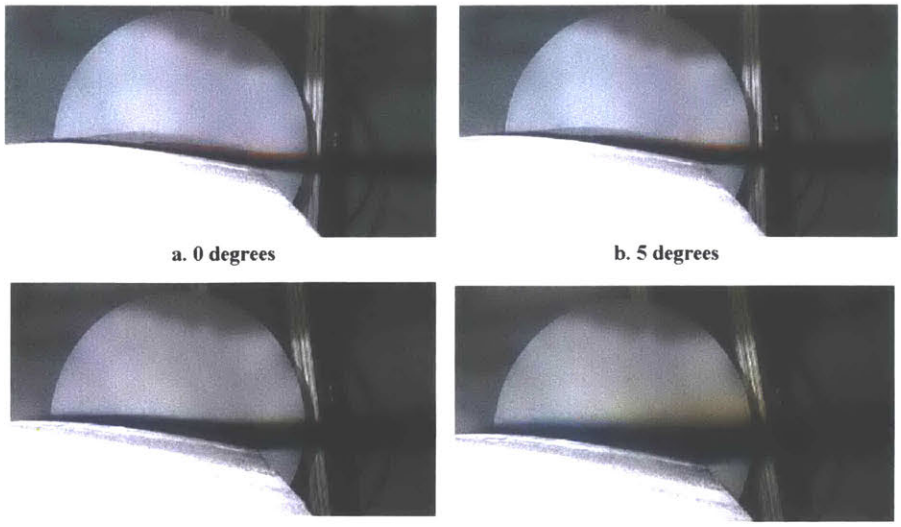

a. 0 degrees

b. 5 degrees

c. 10 degrees

d. 13 degrees

a. NACA0012

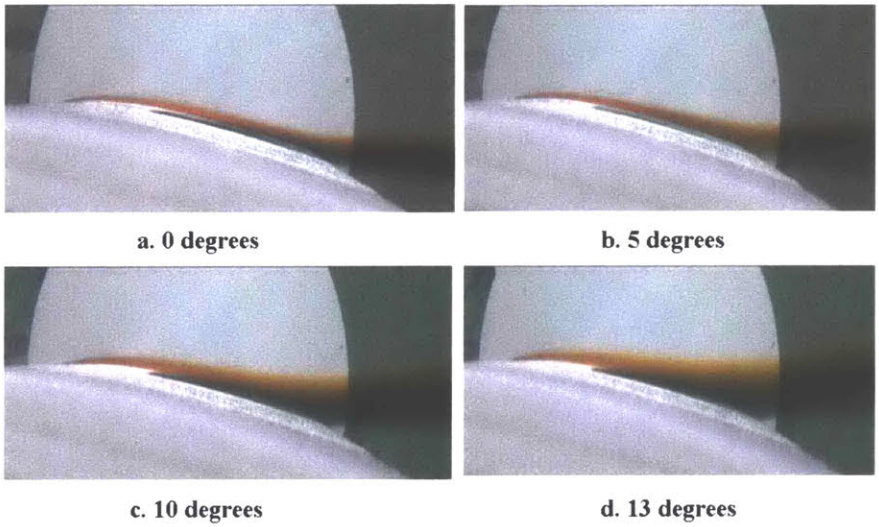

a. 0 degrees

b. 5 degrees

c. 10 degrees

d. 13 degrees

b. NACA0018

Figure 2-3 Boundary layer visualizations for the two wing shapes tested. The increasing angle of attack leads to a larger boundary layer as the point of separation is pushed forward towards the leading edge of the wing. The NACA0012 wing stalled at 12 degrees, and the NACA0018 wing stalled at 16 degrees. The two dye colors in Figure 2-3.b) were utilized to observe the behavior of the boundary layer at around half of the chord length of the wing. Note that the GoPro camera was attached in a way to rotate with the wing, so the change in α is not visually apparent.

To see how the separation points on the wings changed at increasing angles of attack, the angles that the wings were towed at were increased steadily from 0 degrees to the angle where the wing

visually reached stall, 14 for the NACA0012 and 16 for the NACA0018. As a result of the above video analysis, the quantitative thicknesses of the boundary layers that formed at different angles of attack were found. Since the hole that was used in the dye experiment could not be located on the precise front of the wing for mechanical reasons, the measurements start at the location of the first hole, as noted in the figure below.

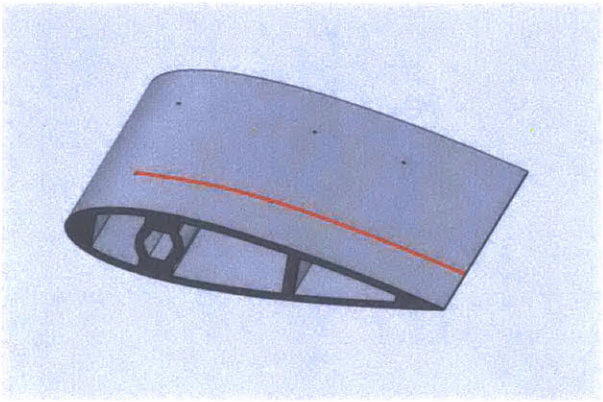

Figure 2-4 CAD model of a portion of the NACA0018 wing. The red line indicates the part of the wing where the boundary layer was measured, starting from the hole closest to the leading edge.

3. Results

3.1 Boundary layer analysis

The results of the tests show an increase in boundary layer thickness as the angle of attack, α, increased from 0 to 13 degrees for both wings, with the NACA0012 wing separating earlier on the wing at lower angles of attack than the NACA0018 wing.

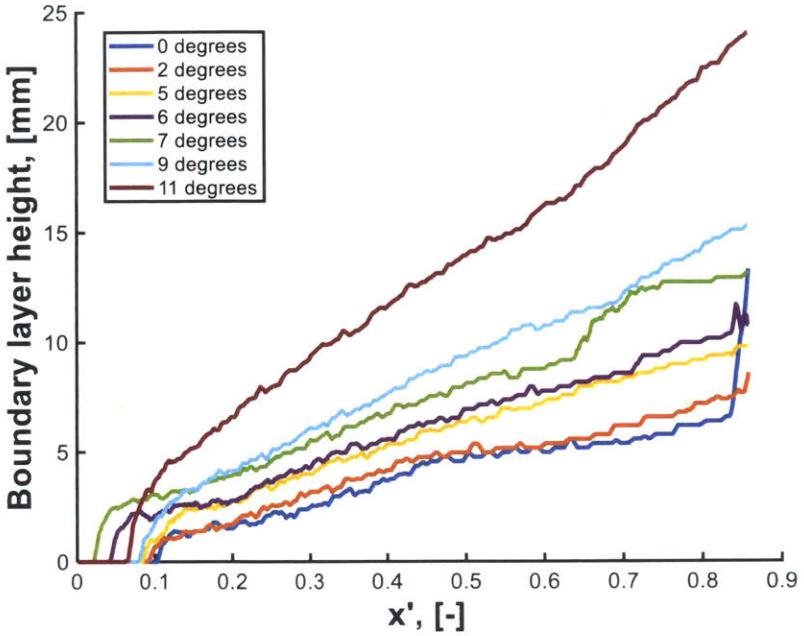

a. NACA0012

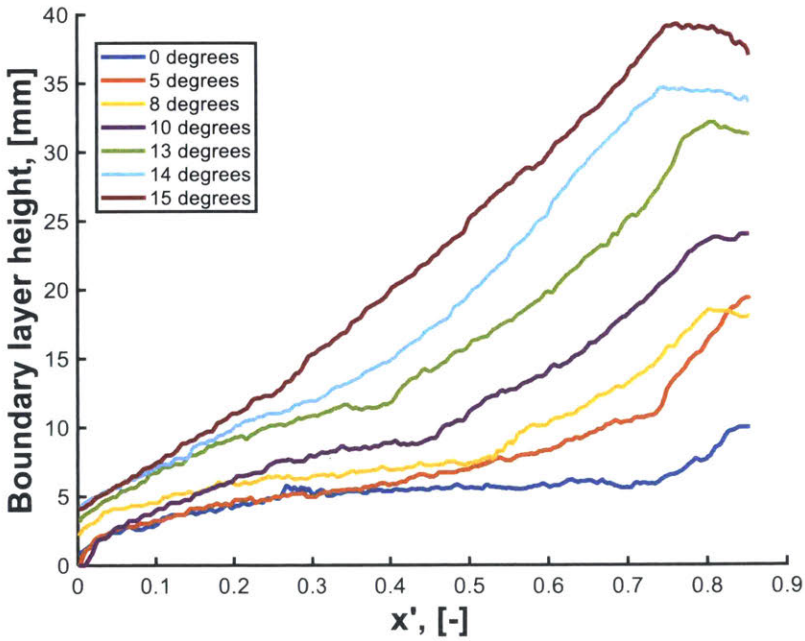

b. NACA0018

Figure 3-1 The non-dimensionalized position on the wing, x', represents the position on the wing as a fraction of the surface length starting from the first point of injection of the dye. The boundary layer height is given in mm at every point along the wing. In general, the boundary layer of the NACA0012 wing increased in thickness more quickly as the angle of attack increased than did the NACA0018 wing. Note that the colors across plots do not correspond to the same angles.

3.2 Point of separation

To see how the boundary layer thicknesses changed over these angles, and to get an idea of the point of separation, there needs to be a baseline measurement of a non-separated boundary layer. As a laminar boundary layer approaches the trailing edge of a flat plate, the thickness increases in accordance to Blasius' solution:

$$\delta \approx 4.91x\sqrt{Re_x}$$

$$Re_x = \rho u_0 x/\mu$$

with $\rho, u_0,$ and μ the density, freestream velocity, and dynamic viscosity of the fluid, respectively, and x corresponding to the position on the plate.

For a streamlined body, the friction drag, or tangential shear stress, experienced is dependent on surface area, and remains essentially unchanged from that of a flat plate. Pressure drag depends on shape, but it only has a large effect on blunt bodies. For an airfoil with a max thickness of less than $\frac{1}{5}$ of the chord length, the friction drag is dominant, and the overall drag can be approximated as that felt by a flat plate of the same size. [16] This approximation is outlined in the figure below, where the NACA0018 wing at $\alpha = 0$ degrees is compared to the Blasius solution.

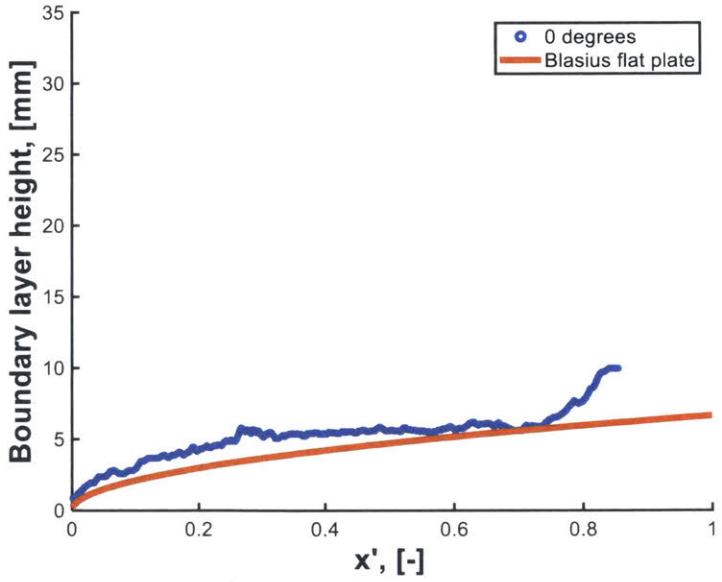

Figure 3-2 The boundary layer height (in mm) corresponding to a non-dimensional location on the wing or plate, x'. For a flat plate in the same conditions as the tested airfoils, the Blasius solution produces similar results to that of actual boundary layer of the airfoil.

The point of separation on the wing can be defined as a rapid increase in boundary layer thickness indicating it has removed itself from the surface of the wing. To define an increase in boundary layer thickness, the proportion of instantaneous height relative to the baseline thickness at 0 degrees is used. An increase of two times the height of the initial boundary layer is the metric used to determine that the boundary layer has separated.

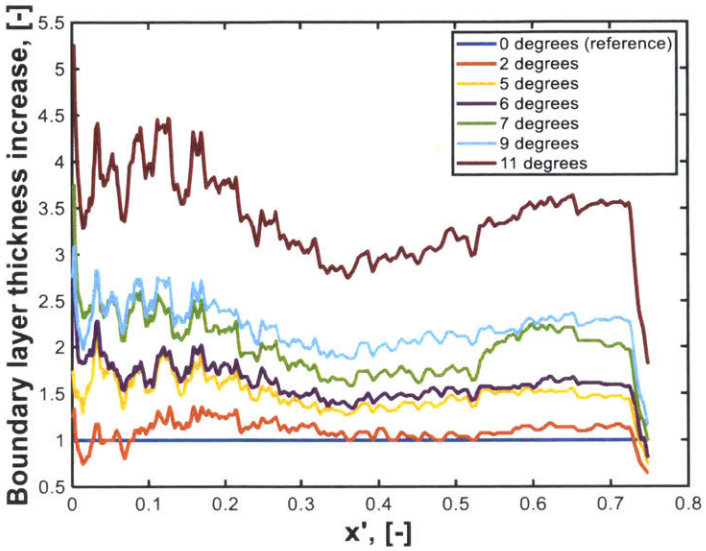

a. NACA0012

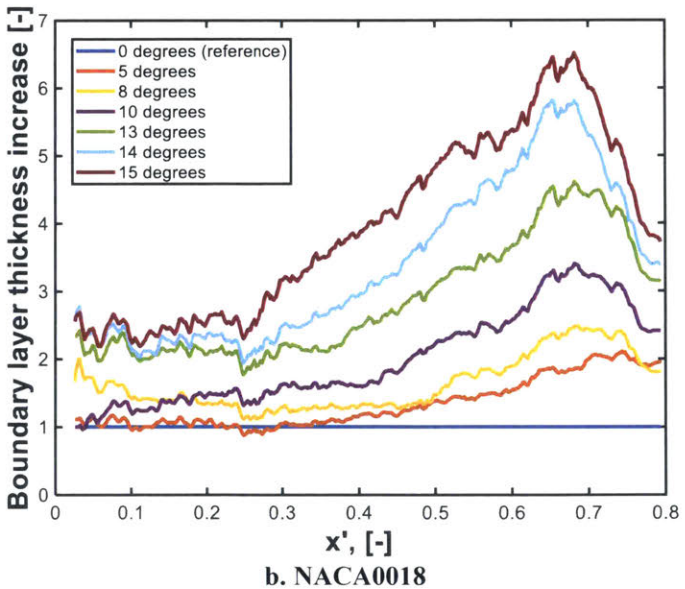

b. NACA0018

Figure 3-3 As the angle of attack increases the overall thickness of the boundary layer increases throughout the length of the wing, normalized by the height of the unseparated boundary layer at $\alpha = 0$.

For the NACA0012 wing this occurred between 5-7 degrees, while NACA0018 separated between 10-13 degrees. The key difference between the two shapes that leads to this difference in performance is that the NACA0012 has a max thickness of 12% of the chord length at 30% of the chord, as opposed to the 18% thickness of the NACA 0018 wing at the same point [17,18]. These ranges, where the boundary layer is just beginning the process of separation, is where the effects of drag reduction will be felt most strongly. At higher angles, the boundary layer will detach from the surface of the wing so early that the moveable surface would need to cover a majority of the wing, and at lower angles the effects of drag are small enough that there is little reduction needed.

The position of the surface can also be roughly determined from these boundary layer plots. To be most effective, it must be present on the wing at the point of separation. This can be seen on the wings as a sudden upward slope in the thickness as the flow travels form the leading to the trailing edge. On the NACA0018 wing, this happens between about 40-60% of the chord length of the wing in the critical range of 10-13 degrees. For the NACA0012 wing, it occurs closer to 50% of the chord length.

3.3 Force measurements

3.3.1 NACA0012

Drag on a wing is composed of many components, including skin friction and form drag, which depend on surface conditions and wing shape, respectively. The drag force can be determined directly through the use of force sensors, which are located at the top and base of the wing throughout the tow tank experiments. In order to put this force into a form where it depends on the shape of the wing as well as the fluid characteristics, the coefficient of drag, C_D, is used,

$$C_D = \frac{D}{\rho A \frac{v^2}{2}}$$

The variable A refers to the frontal area of the wing, and D to the overall drag force. As expected, as the angle of attack increased with the NACA0012 wing, the drag also increased. Through a similar approach, and using the same sensors, the lift generated by the wing can also be found as follows,

$$C_L = \frac{L}{\rho A \frac{v^2}{2}}$$

The lift force, L, can be found directly through measurement. The coefficient of lift increases as the angle of attack increases, then suddenly reaches a point where the separation point has moved close enough to the leading edge that the wing enters a state of stall. This is a quick transition point that is dangerous in aircraft and must be avoided.

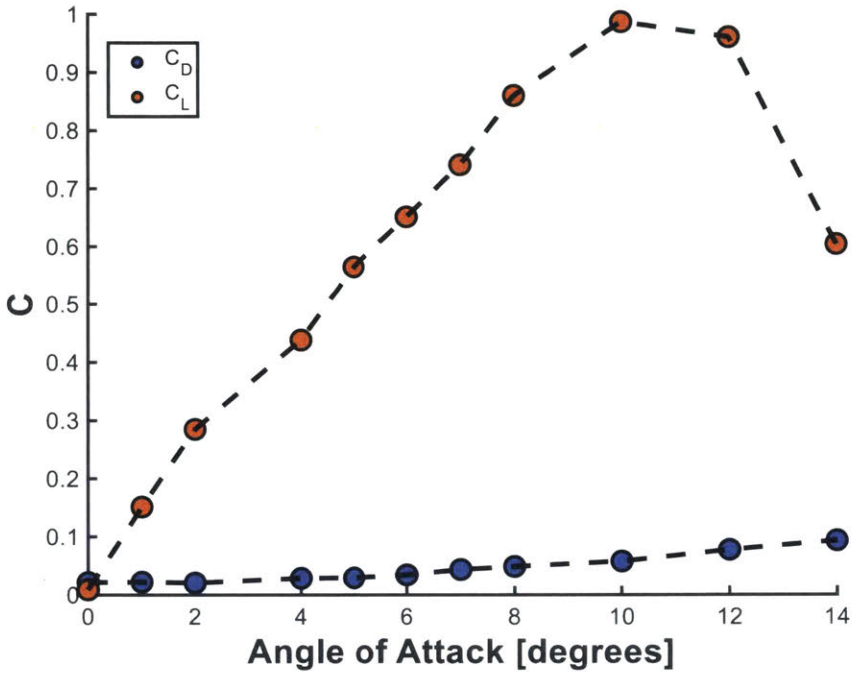

Figure 3-4 As the angle of attack of the wing increases, the lift increases as well, until the eventual point of stall, where the wing can no longer generate a lift force, indicated by a steep, sudden drop in C_L. The data collected by the NACA0012 wing showed exactly this trend, reaching stall around 12 degrees, which matches well with the dye visualization analysis. The drag on the wing, C_D, increases more steadily with α, and continues to increase past the point of stall.

Pushing back the incidence of stall to higher angles of attack is desirable, because the wing is most efficient at these higher angles if stall is avoided. The final point before the effect of separation become overpowering on the NACA0012 wing is at 10 degrees. The angles below this point, in the range from 5-10 degrees, are where the rate of increase in generated lift drops off slightly, again indicating that these angles have the most to gain from the proposed boundary layer control method, as even small increases in lift could potentially move back the onset of stall.

3.3.2 NACA0018

The same measurements and analysis were done with the NACA0018 shape wing. Due to the increased thickness of the NACA0018 airfoil, the boundary layer begins to separate at a higher angle of attack than the thinner NACA0012 airfoil.

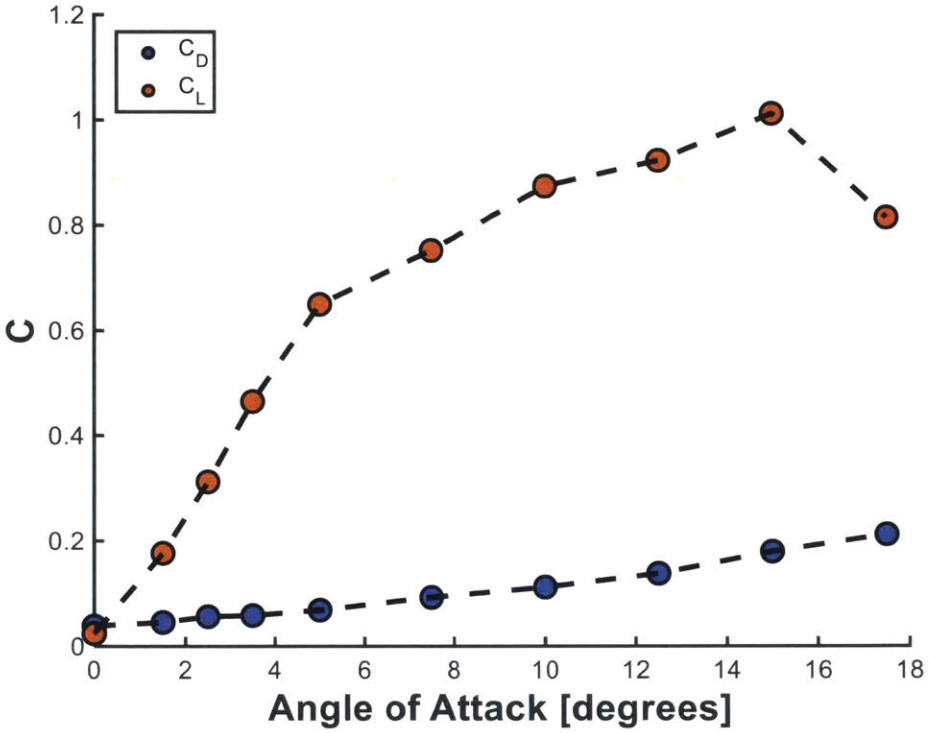

Figure 3-5 The peak of C_L indicates a stall angle around 15 degrees, with a rapid increase as α moves from 0 to 6, and a slower increase from 8 degrees until stall. As with the NACA0012 wing, C_D increases in correlation with the angle of attack, but due to a later incidence of stall for the NACA0018 wing, it reaches higher total drag values.

It is around the 10-12 degree range where the drag begins to increase more rapidly. From the angles of 12 degrees to stall, it was previously shown that the boundary layer separates too close to the leading edge to practically install the moveable surface. However, C_L does not reach a peak until 15 degrees, and stalls soon after.

The coefficients C_D and C_L depend heavily on Reynolds number, and by extension the conditions of the testing environment. Knowing the drag and lift baselines given the current wing shape, water conditions, and freestream velocity will allow direct comparison of future wings under the same shape and conditions, but with an implemented mechanism to push back the point of

separation. A decrease in C_D or increase in $C_L$at the higher angles of attack relative to the current baseline values at the same angles indicates a success in drag reduction.

3.3.3 Predicted values

In order to determine whether the C_D and C_L values found through experimentation were reasonable, the results were compared to the predicted values. The Xfoil: Subsonic Airfoil Development System software, as developed by Mark Drela of MIT, was used to find these predicted values for the same airfoil shapes at Re = $1x10^5$.

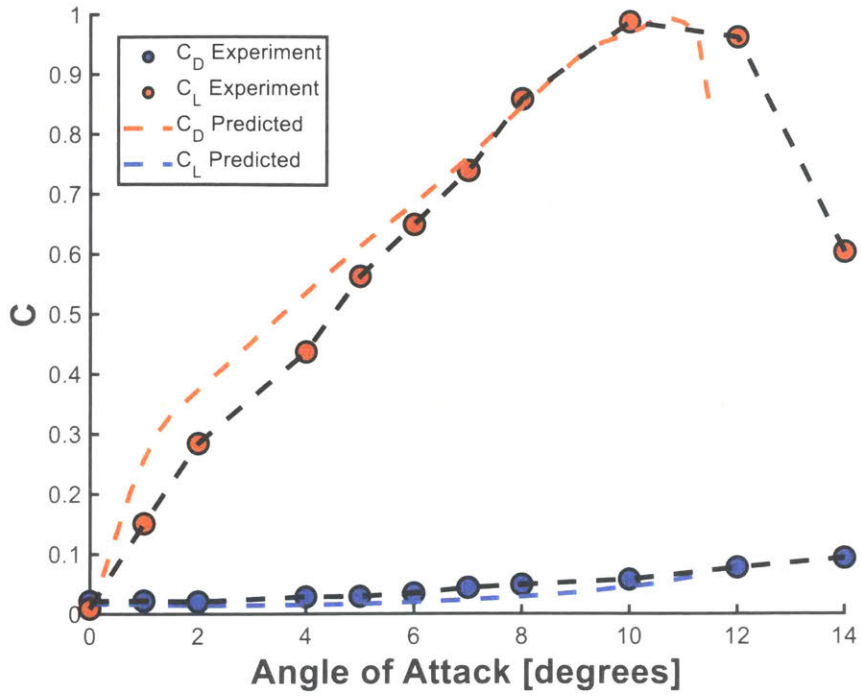

a) NACA0012

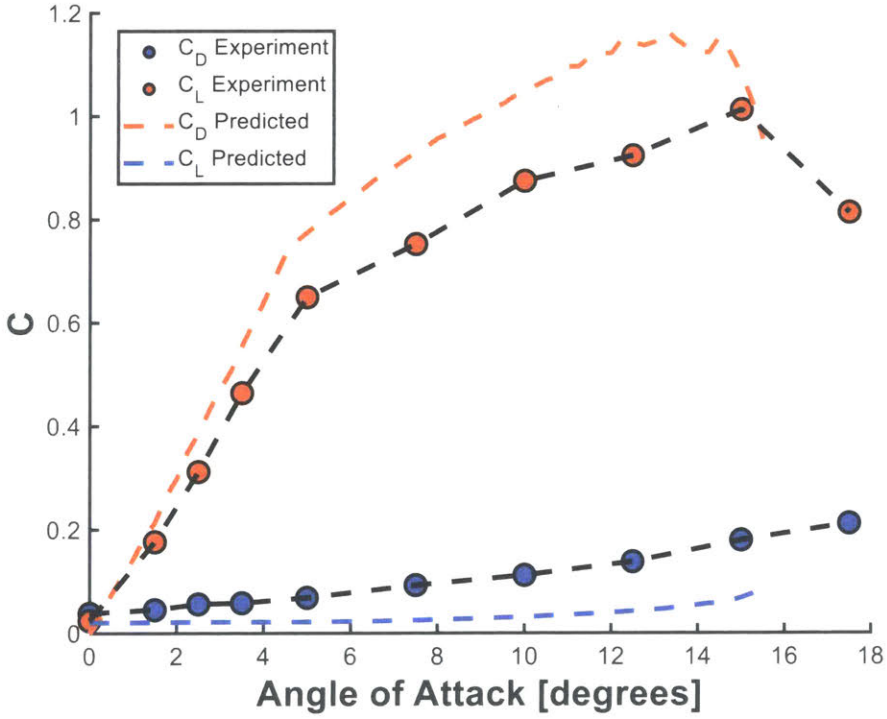

b) NACA0018

Figure 3-6 In the case of both 3-6.a) NACA0012, and 3-6.b) NACA0018, the Xfoil-predicted drag values were lower and the lift values higher than the ones found through experimentation. [17,18]

In both cases, the trends of experimental values follow closely with those of the Xfoil-generated values, and the point of stall for both closely aligns. There are trends in the differences between the two data sets, namely the predicted C_L values are higher than the actual values found in the tank, and the predicted $C_D$values are lower than experimental values. The discrepancy in lift is due to the fact that, although endcaps were installed to mitigate end effects, the airfoil tested in the tank was of finite length, albeit with a larger aspect ratio. Naturally, this generates less lift than that approximated by a wing of infinite span, as in the ideal scenario. The increase in drag in the actual experiments can be explained as other drag effects caused by physically running the tests in the tank, such as the airfoil surface finish and the water conditions, that cannot be estimated through calculation alone.

3.4 Wave parameters

3.4.1 New manufacturing technique

Although critical ranges where separation delay would be most beneficial can be found, the device needed to accomplish this has been incapable of being manufactured thus far. However, a new method of manufacturing by Sam Calisch of the MIT Center for Bits and Atoms looks to address the mechanical concerns stated previously. Instead of making individually actuated flaps to fire in series, or similarly time- and labor- intensive processes to generate a wave motion, this approach involves origami-like construction, where sheets of material are cut and perforated to bend and flex where necessary.

Figure 3-7 Deconstructed view of an early origami prototype for actuated surface. The "origami" constructed sheets (that interface with boundary layer) are

on the far left and right, the carbon fiber sheets with plotted wire is in the middle, and the magnet sheets are in between.
Photos courtesy of Sam Calish, MIT Center for Bits and Atoms

Layers of wire, magnets, and carbon fiber sheets are added in succession, eliminating the need for small, individually moving parts. A Zund 3D plotter is used to carefully lay conductive wire in specific patterns, and stacked with magnets and a protective layer on top.

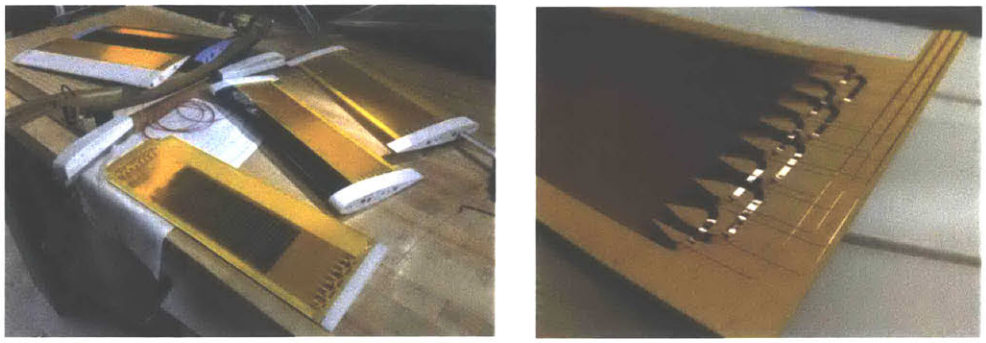

Figure 3-8: *Left* Later prototypes of wings with actuated surfaces. These will be used in future testing.
Right Conductive wire pattern laid out by plotter. The wires are covered in a flexible surface and actuated consecutively moving from leading to trailing edge, initiating a downstream travelling wave (upstream waves are also possible, but not desirable).
Photos courtesy of Sam Calish, MIT Center for Bits and Atoms

When a current is run through the wire coils in an alternating fashion, the perforated sheets allow the surface to move in a travelling wave motion, effectively creating a linear motor. [4] Although the baseline technology is functional, the parameters necessary to effectively push back the point of separation on the wing need to be determined.

3.4.2 Wing characterization

Currently the easiest control method for such a surface is open-loop, with no feedback on the current force measurements or flow conditions on the wing. This method of control inherently introduces operational limitations, as the parameters cannot be effectively adjusted when the wing is in action. In fact, some characteristics such as wavelength are strictly physical properties that must be "hard-coded", and cannot be altered post-manufacturing at all. Since observations of travelling waves have not commonly been conducted on airfoils, key parameters must be estimated and tested to see if flat-plate estimations are sufficient.

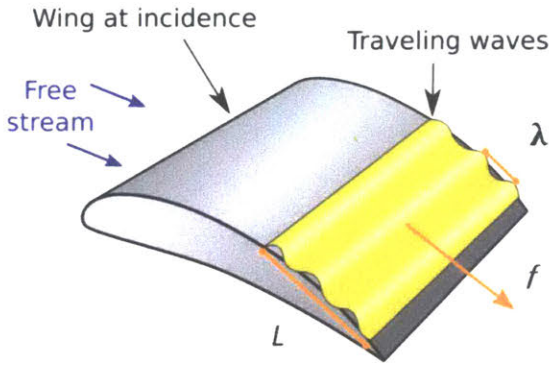

Figure 3-9: Some considerations that must be taken in the design of the wing, including L, the size and location of the surface on the trailing edge, and the wavelength and frequency of the travelling wave, λ and f, respectively. The free stream velocity remains fixed throughout the experiment, and the angle of attack (incidence) has a range of appropriate operating values. Not shown is the wave amplitude, another parameter to take into consideration.
Diagram courtesy of Dixia Fan, MIT Ocean Engineering

The surface location and operating angles determine many of the characteristics of the physical setup, but the parameters of the travelling wave must also be carefully determined, specifically the frequency, wavelength, and amplitude. Frequency is more adjustable post-build, but an initial range must be specified. Amplitude, which also must be controlled in order to prevent unintended separation, is another parameter that must be observed in live testing.

3.4.3 Parameter calculations

The frequency is perhaps the most straightforward to specify, as it is constrained by the limitations of the current manufacturing technology. Currently, the surface is capable of 100 Hz, which will be the basis of calculation for the rest of the parameters. As manufacturing is refined, the parameters can be adjusted using the same relations as the current setup to adapt to different frequencies.

The wavelength and amplitude are linked with the wave speed. Previous studies have shown that a key relation in drag reduction through the use of travelling waves is the ratio of the wave speed to the freestream velocity of the wing. The balance between these two factors can be optimized to generate the highest reduction in drag for the least power expenditure. In a study with a similar Reynolds number conducted by Shen et al., it was found that the ratio of $\frac{c}{U}$ of 1.2 was the most optimal, with c corresponding to the wave speed and U to the freestream velocity, which was 0.7

m/s for these experiments. [3] The wave speed can be related to frequency, f, and wavelength, λ, as $c = \lambda f$. Combining the previous relations,

$$1.2U = \lambda f$$

$$f = 100 \text{ Hz}, U = 0.7 \text{ m/s}$$

$$\lambda \approx 8.4 \text{ mm}$$

Although further testing will be required, for the given frequency an 8.4 mm wavelength is the current optimal dimension.

The amplitude can also be approximated using previous experiments involving downstream travelling waves. The wavenumber, $k = 2\pi/\lambda$, multiplied by the wave amplitude, a, gives a value for wave steepness. Studies have recommended a wave steepness value of around 0.25, which when combined with the approximate wavelength calculated previously gives a recommended amplitude of about 0.3 mm. [1,3,4] This value is likely too small for the capabilities of the surface as it is currently manufactured, which leads to the conclusion that the frequency may need to be decreased in order to raise the amplitude to at least 1 mm. The upper bound of the amplitude, which will be determined best empirically, is important to consider as well.

4. Conclusions

The ideal drag reduction device has already been constructed in nature, and it has quite the head start on all other research in this field. However, recent advances in manufacturing have brought us closer than ever to truly mimicking the movement of fish and other undulatory swimmers, leading us to believe that soon large advancements will be made in wing efficiency.

In order for this promising new technology to be tested and implemented, a standard for comparison needed to be set, and several key parameters had to be determined. Through the course of this study, we have determined that both the NACA0012 and NACA0018 wing shapes hold potential for testing the use of a travelling wave surface, with the baseline C_D and C_L values found for future comparison. The operable ranges of angles of attack was 8-10 degrees and 5-8 degrees for the NACA0018 and NACA0012 wings respectively, and the points of separation for these angles was also found to provide a baseline for future tests, where these points will ideally be moved closer to the trailing edge of the wing. These angles, which are before the wing has completely stalled and after substantial separation has occurred, show where the travelling wave implementation would be most effective. In addition to baseline characteristics of the wing, the

initial operating conditions of the travelling wave were also calculated. These parameters, (λ = 8.4 mm, a =0.3mm, f = 100Hz), can be used to initially determine the effectiveness of the technology, and the exact optimal values can be empirically found from this point.

The processes outlined above will streamline the ability to test the new technology on similar wings, and quickly compare the results to determine its drag reduction capabilities. Future work will include the testing and validation of these parameters on a physical wing in the MIT Towing Tank, and further iterations on the mechanisms that drive the moveable surface.

5. Works Cited

[1] Monokrousos, A., and Brandt, L., "Control of a Separating Boundary Layer with Travelling Waves on the Wall," p. 14.

[2] Anderson, E. J., McGillis, W. R., and Grosenbaugh, M. A., 2001, "The Boundary Layer of Swimming Fish," J. Exp. Biol., **204**(Pt 1), pp. 81–102.

[3] Shen, L., Zhang, X., Yue, D. K. P., and Triantafyllou, M. S., 2003, "Turbulent Flow over a Flexible Wall Undergoing a Streamwise Travelling Wave Motion," J. Fluid Mech., **484**, pp. 197–221.

[4] Calisch, S., Gershenfeld, N., Fan, D., Jodin, G., and Triantafyllou, M., 2019, "Fabrication and Characterization of Folded Foils Supporting Streamwise Traveling Waves," J. Fluids Struct.

[5] Schlichting, H., 1979, *Boundary Layer Theory*, McGraw-Hill Book Company.

[6] Anderson, J. D., 2005, "Ludwig Prandtl's Boundary Layer," Phys. Today, **58**(12), pp. 42–48.

[7] Moghaddam, T., and Neishabouri, N. B., 2017, "On the Active and Passive Flow Separation Control Techniques over Airfoils," IOP Conf. Ser. Mater. Sci. Eng., **248**, p. 012009.

[8] Meksyn, D., 1961, *New Methods in Laminar Boundary-Layer Theory*, Pergamon Press Ltd.

[9] Duan, L., and Choudhari, M. M., "Effects of Riblets on Skin Friction in High-Speed Turbulent Boundary Layers," p. 15.

[10] Bechert, D. W., and Bartenwerfer, M., 1989, "The Viscous Flow on Surfaces with Longitudinal Ribs," J. Fluid Mech., **206**(1), p. 105.

[11] Alexandre, F., 1951, "Aircraft Wing Flap with a Leading Edge Roller."

[12] Bale, R., Shirgaonkar, A. A., Neveln, I. D., Bhalla, A. P. S., MacIver, M. A., and Patankar, N. A., 2015, "Separability of Drag and Thrust in Undulatory Animals and Machines," Sci. Rep., **4**(1).

[13] Fish, F. E., 2006, "The Myth and Reality of Gray's Paradox: Implication of Dolphin Drag Reduction for Technology," Bioinspir. Biomim., **1**(2), pp. R17–R25.

[14] Barrett, D. S., Triantafyllou, M. S., Yue, D. K. P., Grosenbaugh, M. A., and Wolfgang, M. J., 1999, "Drag Reduction in Fish-like Locomotion," J. Fluid Mech., **392**, pp. 183–212.

[15] Kojima, R., Nonomura, T., Oyama, A., and Fujii, K., 2013, "Large-Eddy Simulation of Low-Reynolds-Number Flow Over Thick and Thin NACA Airfoils," J. Aircr., **50**(1), pp. 187–196.

[16] Newman, J. N., 2017, *Marine Hydrodynamics*, MIT Press.

[17] "NACA 0012 AIRFOILS (N0012-Il)" [Online]. Available: http://airfoiltools.com/airfoil/details?airfoil=n0012-il. [Accessed: 04-May-2019].

[18] "NACA 0018 (Naca0018-Il)" [Online]. Available: http://airfoiltools.com/airfoil/details?airfoil=naca0018-il. [Accessed: 04-May-2019].